ARTICLE

Concentration-Dependent Influence of Silver Nanoparticles on Amyloid Fibrillation Kinetics of Hen Egg-White Lysozyme

Wei Fan[a], Xiao-dong Chen[a], Li-ming Liu[a], Ning Chen[a], Xiao-guo Zhou[a*], Zhi-hong Zhang[b*], Shi-lin Liu[a*]

a. Hefei National Laboratory for Physical Sciences at the Microscale, iChEM (Collaborative Innovation Center of Chemistry for Energy Materials), Department of Chemical Physics, University of Science and Technology of China, Hefei 230026, China
b. School of Physics and Optoelectronics Engineering, Ludong University, Yantai 264025, China

(Dated: Received on April 15, 2021; Accepted on April 25, 2021)

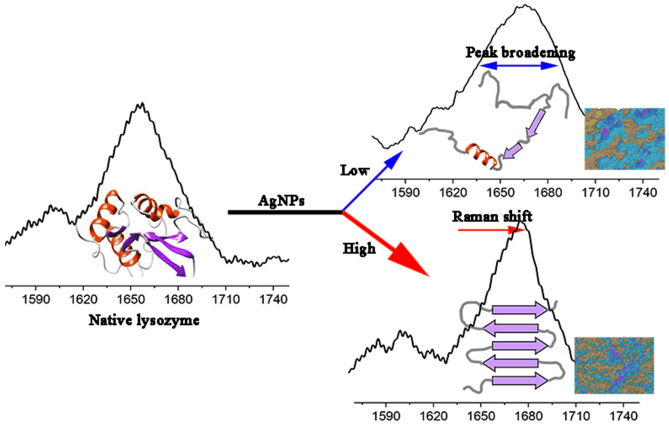

Understanding the influence of nanoparticles on the formation of protein amyloid fibrillation is crucial to extend their application in related biological diagnosis and nanomedicines. In this work, Raman spectroscopy was used to probe the amyloid fibrillation of hen egg-white lysozyme in the presence of silver nanoparticles (AgNPs) at different concentrations, combined with atomic force microscopy and thioflavin T (ThT) fluorescence assays. Four representative Raman indicators were utilized to monitor transformation of the protein tertiary and secondary structures at the molecular level: the Trp doublet bands at 1340 and 1360 cm^{-1}, the disulfide stretching vibrational peak at 507 cm^{-1}, the N-Cα-C stretching vibration at 933 cm^{-1}, and the amide I band. All experimental results confirmed the concentration-dependent influence of AgNPs on the hen egg-white lysozyme amyloid fibrillation kinetics. In the presence of AgNPs at low concentration (17 μg/mL), electrostatic interaction of the nanoparticles stabilizes disulfide bonds, and protects the Trp residues from exposure to hydrophilic environment, thus leading to formation of amorphous aggregates rather than fibrils. However, with the action of AgNPs at high concentration (1700 μg/mL), the native disulfide bonds of hen egg-white lysozyme are broken to form Ag−S bonds owing to the competition of electrostatic interaction from a great deal of nanoparticles. As for providing functional surfaces for protein to interact with, AgNPs play a bridge role in direct transformation from α-helices to organized β-sheets. The present investigation sheds light on the controversial effects of AgNPs on the kinetics of hen egg-white lysozyme amyloid fibrillation.

Key words: Amyloid fibrillation, Silver nanoparticles, Hen egg-white lysozyme, Raman spectroscopy

*Authors to whom correspondence should be addressed. E-mail: xzhou@ustc.edu.cn, apzhz@163.com, slliu@ustc.edu.cn

I. INTRODUCTION

The misfolded protein formed under certain conditions can self-assemble into morphologically similar β-sheet-rich fibrillar aggregates so-called amyloids [1, 2]. These amyloids can induce a series of neurodegenerative diseases such as Alzheimer's disease and Parkinson's disease [3−5]. Temperature and pH are the most common factors associated with fibrillation [6, 7]. Besides, it is interesting that a few small molecules were found to be able to manipulate amyloid formation pathways, *e.g.* folic acid [8], succinimide [9], entacapone [10], and gallic acid oxidation products [11], which provided valuable clues for treatment of the related diseases. Moreover, nanoparticle-containing drugs have attracted widespread interest due to their advantages of being targeted [12−15]. When nanoparticles enter a biological medium, they are exposed to a wide range of proteins and are instantaneously coated to form coronas [16, 17], providing functional surfaces for biomolecules to interact with [18]. However, these nanoparticles themselves also probably have considerable influence on protein denaturation, which are rarely mentioned.

Recently, several reports [17, 19−36] have shown evidences that nanoparticles could affect amyloid fibrillation indeed. Gold nanoparticles were found to be able to induce depolymerization of lysozyme fibrils and reduce cytotoxicity, compared with untreated proteins [20]. Andrea *et al.* reported that iron oxide superparamagnetic nanoparticles functionalized with different amino acids could inhibit lysozyme amyloid fibrillation and uncoil amyloid fibrils [21]. However, an interesting conclusion was drawn by Vácha *et al.*, that the accelerating or inhibiting effects of these nanoparticles on amyloid fibrillation depended on the intrinsic aggregation propensity of Aβ42 peptide or human α-synuclein protein [22].

A similar argument existed for the influence of Ag nanoparticles (AgNPs). Through binding to aggregation prone regions of β-lactoglobulin, AgNPs altered protein aggregation pathways, leading to a morphologic change of aggregates from fibrils to nanorod-like ones [23]. AgNPs capped with citrate could inhibit human islet amyloid polypeptide (IAPP) amyloid fibrillation [24]. However, Gladytz *et al.* found that AgNPs effectively accelerated fibril growth of the NNFGAIL peptide from human islet amyloid polypeptide in physiological aqueous solutions [25]. Following the conclusions, the effects of more nanoparticles on amyloid fibrillation were reported from complete inhibition [26, 27] to obvious acceleration [28, 29], depending on nanoparticle type [30], peptide sequence [31], and physical and chemical conditions [22, 32], such as pH and temperature. Therefore, the diverse effect of each type of nanoparticles on amyloid fibrillation needs a detailed investigation for every protein in specific conditions.

As a model protein, hen egg-white lysozyme (HEWL) has been widely used to study amyloid formation under specific conditions. Structurally, it is a helix-rich protein possessing a high degree of sequence similarity and structural homology to the human variant, which is responsible for hereditary nonneuropathic systemic amyloidosis [37−40]. Thus, it is a cheap but efficient object to study the nanoparticle influence on amyloid formation. Nevertheless, to the best of our knowledge, only a few investigations of AgNPs on the amyloid fibrillation of HEWL have been conducted. Kumar Ban *et al.* observed that starch and polyethylene glycol (PEG) functionalized AgNP might inhibit the amyloid fibrillation and trigger defibrillation process of HEWL effectively [41]. Hassan *et al.* summarized a nanoparticle concentration-dependent influence based on morphologic changes and Thioflavin T (ThT) fluorescence assays [42]. In a solution with concentration higher than 300 μg/mL, AgNPs showed a pattern of dose-dependent induction of aggregation, while an inverse effect was observed in the concentration range of 3−30 μg/mL. However, this conclusion was somewhat contrived in the absence of an interaction study at the molecular level.

Herein, we have performed a combined investigation of the effect of AgNPs on the HEWL amyloid fibrillation under thermal and acidic conditions (65 °C and pH=2.0). Two representative concentrations of nanoparticles were selected, 17 μg/mL for the low concentration and 1700 μg/mL for the high one. Besides morphologic changes observed using atomic force microscopy (AFM), the incubation time-dependent Raman spectroscopy of aqueous HEWL was recorded during amyloid fibrillation. The secondary and tertiary structural transformations of HEWL were clearly detected at the molecular level. Finally, the action mechanisms of AgNPs at different concentrations were revealed by analyzing kinetics of the specific Raman markers.

DOI:10.1063/1674-0068/cjcp2104069

II. MATERIALS AND METHODS

A. Preparation of Ag nanoparticles and HEWL solutions

Silver nitrate ($AgNO_3$) and sodium citrate were purchased from Sinopharm Chemical Reagent Co. Ltd. AgNPs were synthesized according to the well-known Turkevich method [43−45]. Briefly, a solution of $AgNO_3$ ($\sim 1.0\times10^{-3}$ mol/L) in deionized water was heated to boil under vigorous stirring. Sodium citrate solution was added drop-wise to the $AgNO_3$ solution as soon as the boiling commenced. The color of the mixture slowly turned into yellow-green, indicating the reduction of the Ag^+ ions. Heating was continued for an additional 15 min, and then the solution was cooled to room temperature before employing for further experimentation. The characteristic of AgNPs was verified using the UV-Vis absorption spectrum of their hydrosols. A high plasmon peak at ∼428 nm in FIG. S1(a) of the supplementary materials indicated that the average diameter of nanoparticles is ca. 70 nm [46]. In addition, SEM micrographs confirmed that these AgNPs were well dispersed, and were near spherical (FIG. S1(b) in supplementary materials).

HEWL (activity: 22800 U/mg) was purchased from Sangon Biotech (Shanghai) Co. Ltd., and was used without further purification. Amyloid fibrillation of the lysozyme was prepared under thermal and acidic conditions (65 °C and pH=2.0) as described in Refs.[9, 47−49]. Briefly, three types of aqueous HEWL solutions (20 mg/mL) were prepared in the absence or presence of AgNPs, where the concentration of nanoparticles were 17 and 1700 μg/mL, respectively. The pH value of solutions was adjusted to 2.0 with the addition of hydrochloric acid, since chloride ions showed very little influence on protein structures [50−52]. The prepared lysozyme solutions were sealed in glass vials, and were incubated in a thermoshaker incubator at 65 °C without agitation. At specific incubation time, aliquot of the fibril-forming solution was taken out from the glass vial, and the gelatinous phase was separated by centrifugation at 12000 g for 20 min. Aliquots of the supernatant were directly used for ThT fluorescence assay, AFM, and Raman spectroscopy.

B. Spontaneous Raman spectroscopy

The spontaneous Raman spectroscopy was performed as described elsewhere [49, 53−57]. Briefly, a continuous-wave laser at 532 nm (Verdi V5, Coherent) with a power of 4 W was focused on the solutions in a 10 mm×10 mm quartz cuvette by an f=5 cm lens. The confocal Raman scattering was dispersed by a triple monochromator (Triple-Pro, Acton Research), and was detected using a liquid-nitrogen-cooled CCD detector (Spec-10:100B, Princeton Instruments) to record Raman spectra. Raman shifts were carefully calibrated using standard spectral lines of a mercury lamp. The acquisition time for recording each spectrum was approximately 1 min, with a resolution of about 1 cm^{-1}. Under the same conditions, Raman spectra at every incubation time were accumulated and averaged by 20 acquisitions. Finally, the average Raman spectra were corrected by subtracting the spectra of hydrochloric acid solution measured under identical conditions.

C. Atomic force microscopy (AFM)

Protein solutions were diluted 100-fold with Milli-Q water, and were dropped on a freshly cleaved mica at room temperature. The mica was rinsed 5 times with deionized water, and was dried with nitrogen gas. Using a Veeco DI-MultiMode V scanning probe microscope, the AFM images of samples were recorded in the tapping mode using a 5 μm×5 μm scanner. All AFM images were processed using the open-access software from Nanoscope Inc.

D. ThT fluorescence assays

ThT was purchased from Sinopharm Chemical Reagent Co. Ltd, and was used without further purification. Protein solutions were diluted 10-fold with the ThT solution ($\sim 1\times10^5$ mol/L). During HEWL amyloid fibrillation, 40 μL aliquots of the supernatant were picked up from vials after various incubation time, and were added to 960 μL ThT solutions. Using an excitation wavelength of 440 nm, fluorescence emission within the wavelength range of 400−800 nm was dispersed and detected with a monochromator (TriplePro, Acton Research) equipped with a photomultiplier (R928, Hamamatsu). Fluorescence assays were performed *ex situ* for the solutions immediately under ambient condition. Five acquisitions were averaged to obtain the fluorescence intensity at each specific incubation time.

DOI:10.1063/1674-0068/cjcp2104069

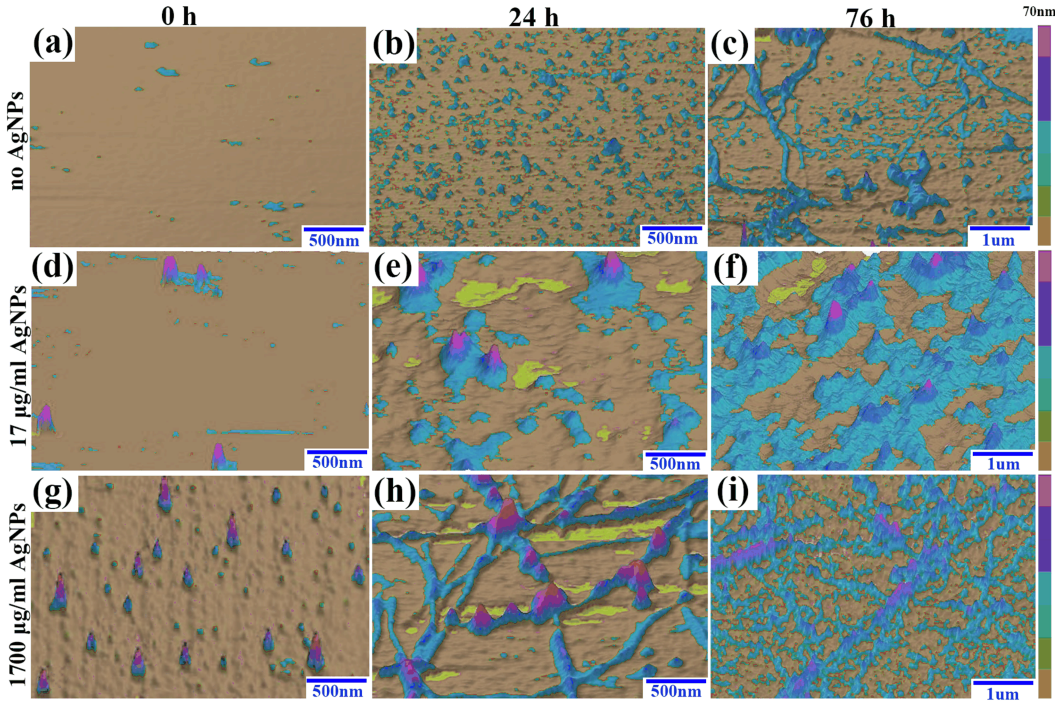

FIG. 1 AFM 3D surface images of HEWL solutions (pH=2.0) incubated at 65 °C for (a) 0 h, (b) 24 h, (c) 76 h in the absence of NPs. For comparison, AFM images of HEWL in the presence of Ag NPs (17 μg/mL) incubated under the identical conditions for (d) 0 h, (e) 24 h, (f) 76 h, as well as those for (g) 0 h, (h) 24 h, (i) 76 h in the presence of Ag NPs (1700 μg/mL).

III. RESULTS AND DISCUSSION

A. Morphologies of HEWL during amyloid fibrillation

FIG. 1 shows the AFM images of HEWL in the absence and presence of AgNPs, at three kinds of representative incubation time, in which the morphological changes of protein can be distinctly observed. No particles were observed in the AFM images at the very early stage (FIG. 1(a)), since the native lysozyme was too small in size. In the absence of nanoparticles, nearly spheroidal oligomers were gradually formed after incubation for 24 h (in FIG. 1(b)), while a small number of short protofibrils of ∼7 nm in diameter were found after incubation for 76 h (FIG. 1(c)). All images are consistent with the previous results under thermal and acidic treatment [9, 49, 58].

In the presence of AgNPs with the low concentration of 17 μg/mL, more amorphous aggregates were gradually formed with incubation time of 76 h (FIG. 1(f)), in comparison with FIG. 1(c). However, to our surprise, no protofibrils were observed after incubation for 76 h (in FIG. 1(f)), thus concluding that AgNPs with the lower concentration might be an efficient suppressor for amyloid fibrillation. This phenomenon was consistent with the Hassan *et al.*'s observation [42]. In contrast, a few palpable differences were observed in the AFM images of HEWL in the presence of AgNPs with the high concentration of 1700 μg/mL. After incubation for 24 h, some dispersed fibril-bridged AgNPs were clearly found in FIG. 1(h), as well as some short protofibrils with a diameter of ∼7 nm, indicating that the amyloid fibrillation of HEWL was obviously accelerated. Moreover, after incubation for 76 h, a great deal of the fibril-bridged AgNPs even coalesces to form linear nanoparticle assemblies, as shown in FIG. 1(i). Therefore, the morphological change of HEWL seems to validate the previous conclusions [42], that AgNPs with the high concentration can promote the amyloid fibrillation of HEWL.

B. Raman spectroscopy of HEWL during amyloid fibrillation

Raman spectroscopy is powerful to detect the secondary and tertiary structure transformations of protein, since Raman shift, scatting intensity, and full width at half-maximum (FWHM) of some specific vi-

DOI:10.1063/1674-0068/cjcp2104069

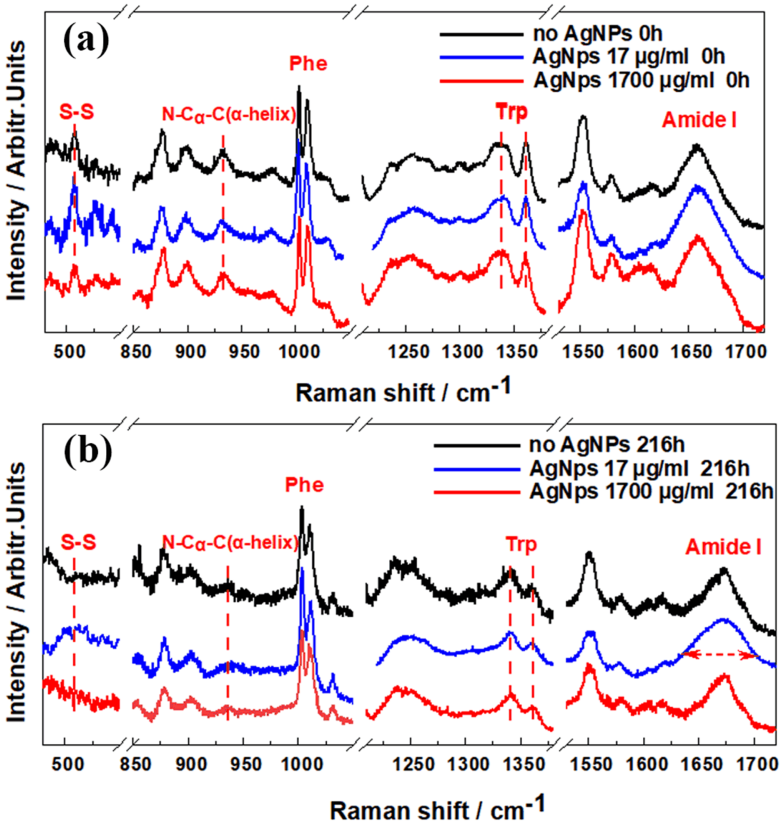

FIG. 2 Raman spectra of HEWL aqueous solutions under thermal (65 °C) and acidic (pH=2.0) conditions, in the absence and presence of AgNPs at the two concentrations (17 and 1700 μg/mL), recorded at (a) 0 h and (b) 216 h. The spectral intensities were normalized by the Phe band at 1003 cm^{-1}.

brational bands are highly sensitive to the microenvironment of protein [59−61]. As noted previously [9, 49, 58], four well-known vibrational bands of protein were selected to quantitatively describe the HEWL structure changes during amyloid fibrillation: (i) the N-Cα-C stretching vibration of skeleton at 933 cm^{-1} is associated with α-helical structures [60, 62, 63]; (ii) the amide I band at 1640−1680 cm^{-1} is contributed by various secondary structures, *i.e.* α-helical structures usually have low-frequency accordion-like vibrations at 1640−1660 cm^{-1} [64, 65], organized β-sheets contribute to 1660−1680 cm^{-1} [66−68], and disordered structures such as β-turns, loose β-strands, and polyproline structures (so-called "random coils") have the vibrational frequency lower than 1640 cm^{-1} or higher than 1680 cm^{-1} [60, 65]; (iii) the Fermi doublet peaks at 1340 and 1360 cm^{-1} are correlated to the hydrophobic/hydrophilic environments around tryptophan (Trp) indole ring [49, 69]; (iv) the stretching vibrational band of disulfide (SS) bonds is located at 507 cm^{-1} [59, 69, 70].

The Raman spectra of native and denatured HEWL were recorded in the region from 440 cm^{-1} to 1760 cm^{-1}. Compared with that of the native lysozyme, all band intensities of the denatured protein were much weaker, because protein concentrations in the supernatants decreased apparently due to fibril formation and gelation. As indicated previously [71−73], the Raman scattering of Phe ring at 1003 cm^{-1} was insensitive to its microenvironment, and was proportional to protein concentration. Thus, the recorded Raman scatting intensities were normalized by this Phe peak intensity. To directly show the AgNPs influence on protein molecular structure in the native and denatured states, FIG. 2 plots the spectra recorded at 0 h and 216 h in the absence and presence of AgNPs at two concentrations (17 and 1700 μg/mL), respectively, where the 216 h incubation time was long enough to complete amyloid fibrillation of HEWL as indicated in our previous study [9, 49, 58].

At the very early incubation stage like 0 h, only disulfide stretching vibrational band showed evident changes

DOI:10.1063/1674-0068/cjcp2104069

with the action of AgNPs among the four spectral markers (FIG. 2(a)). To our surprise, this band intensity at the low concentration (17 μg/mL) was higher than that with the absence of nanoparticles. According to that the disulfide bonds play the stabilizer role in protein structure [74], the enhancement of this band intensity indicates that AgNPs can provide an extra stable environment for proteins prior to hydrolysis. However, when the nanoparticle concentration was increased to 1700 μg/mL, a visibly reduced disulfide peak at 507 cm^{-1} was observed in contrast with its intensity in the native state without nanoparticles, indicative of a role of denaturation accelerator. This contradictory effect could be explained in the view of electrostatic interactions. Electrostatic interaction between nanoparticles and proteins is of considerable importance in the design of nanoparticles that capture, neutralize, and deliver target molecules in a biological milieu [75]. Under the present experimental conditions, the surfaces of nanoparticles were coated by negative charges [76, 77]. The electrostatic interaction naturally attracted those positively charged amino acid residues on the nanoparticle surface, stabilizing the protein structure. Thus, the Ag−S bonds were formed between the AgNP surface and the thiol-bearing cysteine residues formerly involved in disulfide bonding [78]. On the contrary, at the high AgNP concentration a positively charged amino acid residue near the disulfide bonds could simultaneously interact with multiple nanoparticles, and then the competition between these electrostatic interactions might weaken and destroy the disulfide bond, leading to the instability of the protein structure. Consequently, AgNPs became denaturation accelerators in this case.

Compared with FIG. 2(a), the Raman spectra of denatured HEWL (FIG. 2(b)) showed evident changes for all four markers, *e.g.* reductions of N−Cα−C stretching and disulfide stretching peaks, increase of Trp doublet peak intensity ratio I_{1340}/I_{1360}, and blue-shift of amide I peak. The incubation time-dependent spectral markers will be discussed in detail in the following section, to show step-by-step transformation mechanisms. Herein, we would like to pay attention to the spectral differences of denatured protein with the action of AgNPs, in comparison to the mature fibrils formed under thermal and acidic conditions without nanoparticles. Apparently, both N-Cα-C stretching and disulfide bonds stretching peaks almost disappeared after a long-time incubation, regardless of the existence of nanoparticles, indicating that the α-helical secondary structures were completely transformed. Moreover, a much broadened amide I peak was observed with the action of AgNPs at low concentration, while the narrower peak profiles were found in the absence and presence of AgNPs at high concentration (FIG. 2(b)). According to that the amide I band involves spectral contributions of various secondary structures, the wider band profile implies disorganized structures of aggregates, which generally agrees well with the observations in AFM images.

C. Unfolding kinetics of HEWL tertiary structure during amyloid fibrillation

As previously reported [9, 49, 58, 79], the HEWL amyloid fibrillation is a typical multi-stage transformation mechanism. To further explore the exact influences of AgNPs on each stage of amyloid fibrillation, kinetics of specific structure transformation were investigated by recording incubation time-dependence spectra of the corresponding Raman markers. FIG. 3(a) shows the dependent curve of the I_{1340}/I_{1360} ratio. It is well known that this Fermi resonance consists of the fundamental in-plane N−C stretching mode and combination bands of the ring out-of-plane vibrations of the Trp residue [60, 65, 69]. Thus, the I_{1340}/I_{1360} ratio is a sensitive probe for studying hydrophobic/hydrophilic environments around the Trp indole ring. If I_{1340}/I_{1360} is less than 1, the indole ring is in a hydrophobic environment or in contact with the aliphatic side chains, on the contrary, the indole ring is located in a hydrophilic environment or exposed to an aqueous medium [69, 80].

Overall, the I_{1340}/I_{1360} ratio gradually increased with incubation time, regardless of the existence of nanoparticles, which agreed with the exposure of Trp residues on HEWL side chain to hydrophilic environment. However, it is interesting to observe completely different influences of AgNPs at high and low concentrations. In comparison to the exposing rate of Trp groups without nanoparticles, AgNPs at the high concentration slightly accelerated the Trp exposure, but the final states eventually converged, as shown in FIG. 3(a). This trend is consistent with the above morphological changes and the formation of mature fibrils. However, AgNPs at the low concentration exhibited an unexpected mitigation effect for the Trp exposure, since the I_{1340}/I_{1360} ratio only slightly increased in FIG. 3(a). This influence like a stabilizer can be due to the electrostatic interaction

DOI:10.1063/1674-0068/cjcp2104069

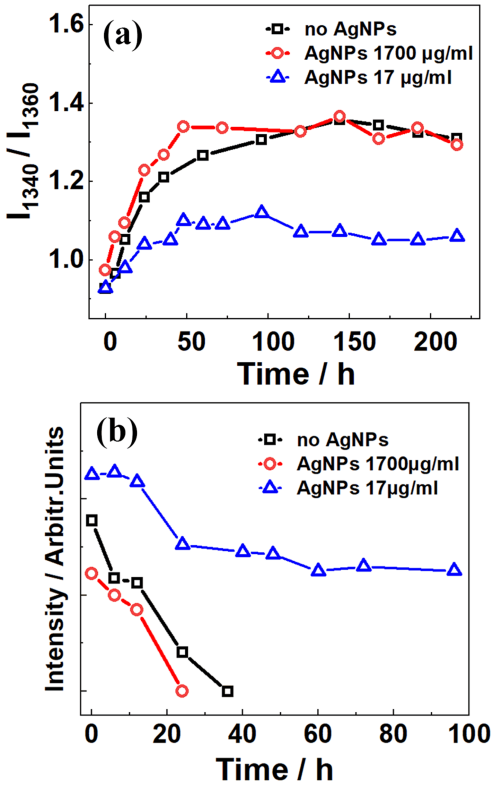

FIG. 3 (a) Incubation time-dependent curves of the I_{1340}/I_{1360} ratio and (b) the disulfide bonds stretching band intensity at 507 cm^{-1}.

between the positively charged amino acid residues and the nanoparticle surfaces. For comparison, the incubation time-dependent curve of the disulfide stretching band intensity at 507 cm^{-1} is plotted in FIG. 3(b). Apparently, its kinetic process was entirely consistent with that of the I_{1340}/I_{1360} ratio under three experimental conditions. Therefore, all evidences strongly suggest the concentration-related effect of AgNPs on the early stage of HEWL amyloid fibrillation, which depends on the competition between the electrostatic interaction and the disulfide bond. In addition, as indicated in FIG. 3, the tertiary structures of HEWL were dominantly denatured within 50 h under the present three treatments, however, more than a half disulfide bonds and Trp residuals remain their original states with the action of AgNPs at the concentration of 17 μg/mL.

D. Transformation kinetics of HEWL secondary structures

To form mature amyloid fibrils, the α-helices of HEWL in the native state need be completely transformed to the organized β-sheet-rich structures. Thus, two Raman markers, the N−Cα−C band intensity at 933 cm^{-1} and the peak position of amide I band, were utilized to monitor this transformation kinetics of protein secondary structure during amyloid fibrillation. As indicated previously [59, 60, 67, 69, 81, 82], the N−Cα−C intensity is proportional to the population of α-helices, while the amide I band consists of the contributions from various secondary structures of protein. Depending on the strength of the hydrogen bonding interaction (C=O$\cdots$H), which involve amide groups and the dipole-dipole interaction between carboxyl groups, the specific secondary structures have different Raman frequencies. Therefore, the amide I peak position was widely used as a sensitive spectral probe for protein secondary structures, especially α-helices and β-sheets. FIG. 4 shows the incubation time-dependence of these two specific Raman bands.

For the N−Cα−C band, its intensity was monotonously reduced to the minimum at an approximately same rate within early incubation time of ∼50 h, regardless of the existence of AgNPs, indicating that AgNPs have insignificant influence for uncoiling of the α-helices in comparison to the thermal and acidic treatment. However, the completely different kinetics was observed for the blue-shift of the amide I peak position in the absence and presence of nanoparticles, as shown in FIG. 4. With the absence of nanoparticles, the curve displayed a sigmoid functional relationship (FIG. 4(a)), indicative of a typical two-state transformation mechanism under thermal and acidic conditions [79], in which protein aggregation endured a lag phase (∼20 h), followed by a rapid growth (20−100 h) and an equilibrium phase (>100 h). The time delay between the formation of β-sheets and the reduction of α-helices exactly validated that the destruction of α-helices prefers to form random coils, and thermal diffusion mediated the gradual formation of hydrogen bond networks of the organized β-sheets, prior to assembling to protofibrils [49].

With the action of AgNPs at low concentration, a ca. 20 h lag time still remained as shown in FIG. 4(b), but the growing phase was dramatically accelerated. After incubation for 50 h, the amide I band position was further unchanged. This acceleration effect was more visibly observed at the high nanoparticle concentration, even leading to apparent disappearance of the lag phase (FIG. 4(c)). It is worth noting that compared with the reduction of the N−Cα−C band intensity, the almost identical kinetic rates indicate the conformational trans-

DOI:10.1063/1674-0068/cjcp2104069

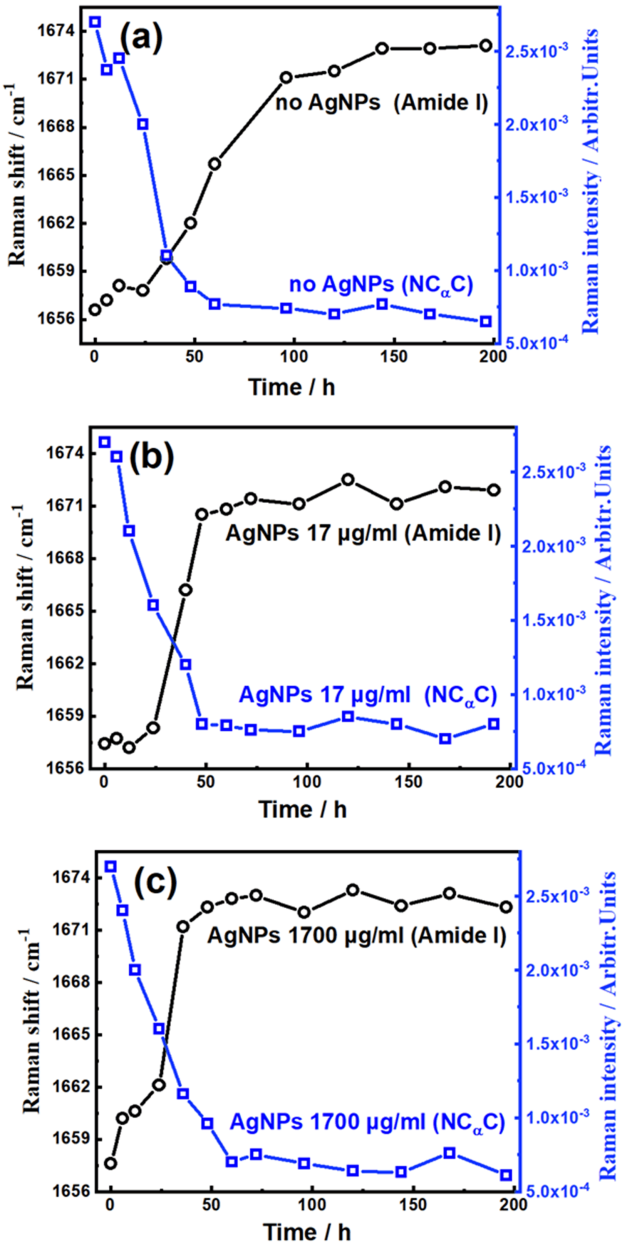

FIG. 4 Incubation time-dependent curves of the N-Cα-C stretching band intensity at 933 cm^{-1} and the peak position of the amide I band, in the absence (a) and presence of AgNPs at the concentrations of (b) 17 μg/mL and (c) 1700 μg/mL.

formation from α-helices to β-sheets occurs synchronously. On the surfaces of AgNPs, the ionic electrostatic forces concomitantly attract those positive amide residues in the backbones of the surrounding peptide strands, thus this relatively organized structure naturally accelerates the formation of hydrogen bond networks of β-sheets. In other words, AgNPs play a bridge role to promote direct transformation of α-helices to organized β-sheets by skipping the formation of intermediary random coils.

In addition, the blue-shift of the amide I peak position was almost as the same as 13 cm^{-1} with the three treatments, as shown in FIG. 4. Such a shift seems to indicate that the dominant secondary structures of denatured HEWL are transformed to organized β-sheets. However, the spectral profile of the amide I band after incubation for 216 h exhibited visibly different with the action of AgNPs at low and high concentrations, as shown in FIG. 2. Thus, the incubation time-dependent Raman spectra in the amide I wavenumber range under the three experimental conditions were expected to be different and thus were compared in FIG. 5. Apparently, the band profile changes in the absence and presence of AgNPs in different concentrations showed some considerable distinctions, besides a faster transformation rate induced by the high concentration nanoparticles. In comparison to the case without nanoparticles, the band with AgNPs at the low concentration of 17 μg/mL remained a much wider profile after incubation for 24 h. Especially, the high-wavenumber tail (>1680 cm^{-1}) and the low-wavenumber part (<1640 cm^{-1}) in FIG. 5(b) maintained throughout relatively considerable population ratios, verifying the formation

DOI:10.1063/1674-0068/cjcp2104069

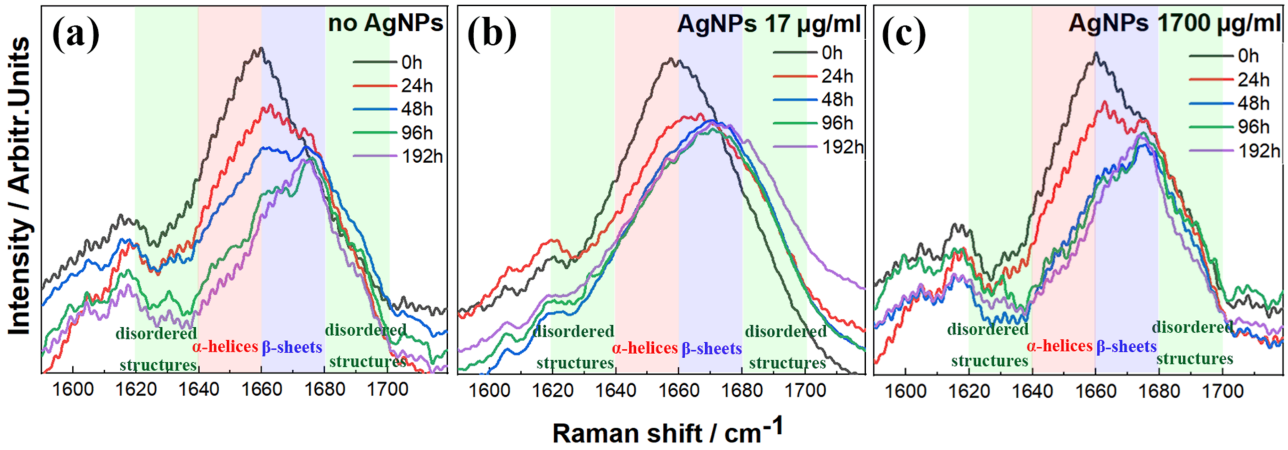

FIG. 5 Incubation time-dependent spectra of HEWL in the amide I wavenumber range, in the absence (a) and presence of AgNPs at the concentrations of (b) 17 μg/mL and (c) 1700 μg/mL.

of random coils with disordered structures suggested by the AFM images. However, in the presence of AgNPs at the high concentration (1700 μg/mL), the change of the amide I band profile during this whole incubation process was very similar to that without nanoparticles, except for a faster transformation rate. This consistency agrees with the predominant formation of amyloid fibrils rather than amorphous aggregates, as seen in AFM images.

Due to spectral overlapping of various secondary structures in amide I band, it is difficult to quantitatively identify the contributions of β-sheets using Raman spectroscopy. Thus, the ThT fluorescence assays were used to further check the formation kinetics of organized β-sheets during amyloid fibrillation. Since the ThT fluorescence intensity at 480 nm increases significantly as a result of ThT specially binding to β-sheet structure, this fluorescence intensity is widely used as the gold standard for selective staining and quantification of the formation of organized β-sheet structures [83, 84]. FIG. 6 shows the fluorescence spectra of HEWL/ThT solution in the absence and presence of AgNPs at two specific incubation times (*i.e.* 0 and 144 h), and the corresponding kinetics of the ThT fluorescence intensity at 480 nm were plotted in FIG. 6(b).

At the early stage of incubation, ThT fluorescence intensity of native lysozyme was very weak, owing to the very limited population of organized β-sheets in HEWL solutions. Then the fluorescence was gradually enhanced over incubation time, due to the formation of more and more organized β-sheet structures. In the absence of AgNPs, the fluorescence intensity was approximately saturated after incubation for 144 h, as the mature fibrils were formed. Interestingly, unlike the three-stage mechanism suggested by a representative sigmoid functional relationship, the detailed incubation time-dependent curve in FIG. 6(b) (black trace) clearly shows a four-stage process: during the first 20 h, the fluorescence rapidly increased to nearly a quarter, and then maintained until 100 h; it reached the maximum at ∼120 h after proceeding a secondary growth phase.

Regardless of the existence of AgNPs, the kinetics in the first stage was apparently identical as shown in FIG. 6(b), as the dominant changes for protein structure were exposing aromatic side chain amino acids to water and uncoiling of the α-helices. This independent behavior agrees with the above conclusion that AgNPs only have very limited influence on these structural transformations. However, AgNPs exhibited a role of accelerator for the enhancement of ThT fluorescence at the second stage, which perfectly agreed with their bridge roles to promote direct transformation of α-helices to organized β-sheets without forming intermediary random coils. Actually, on the surfaces of nanoparticles, the ionic electrostatic forces attract the positive amide residues in the backbones of the surrounding peptide strands, thus this relatively organized structure naturally accelerates the formation of hydrogen bond networks of β-sheets.

To our surprise, the acceleration effect of AgNPs seemed to be suspended after incubation for ∼50 h, at the high concentration (1700 μg/mL). It is worth noting that at present the ThT fluorescence intensity

DOI:10.1063/1674-0068/cjcp2104069

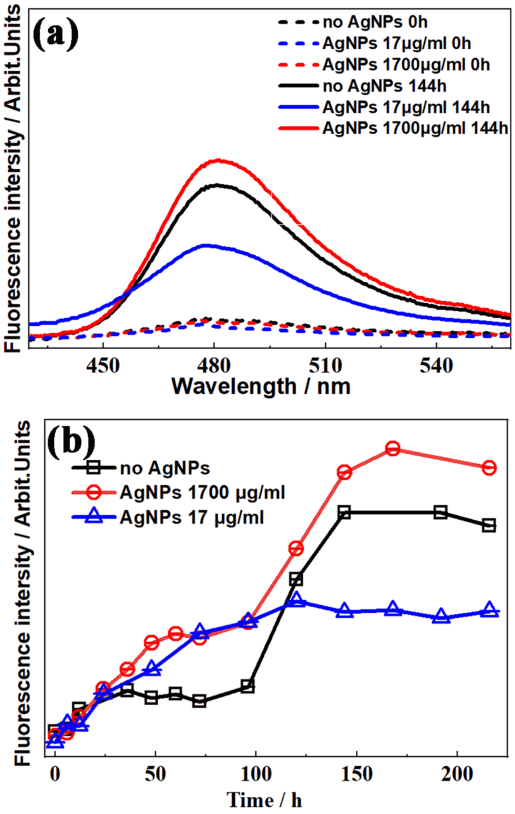

FIG. 6 (a) ThT fluorescence spectra of HEWL/ThT solution at two incubation times, in the absence (in black) and presence of AgNPs at the concentrations of 17 μg/mL (in blue) and 1700 μg/mL (in red). (b) Incubation time-dependence of the ThT fluorescence intensity at 480 nm.

approximately equals to that at the low concentration (17 μg/mL). As indicated in FIG. 1 of AFM images, many amorphous aggregates were formed and no protofibrils were observed with incubation time, with the action of AgNPs at low concentration. Thus, the competition between the formation of amorphous aggregates and protofibrils with organized β-sheet-rich structure reduced the growth rate of ThT fluorescence. After incubation for 100 h, the fluorescence was remarkably enhanced under the condition of nanoparticle at high concentration (red trace in FIG. 6(b)), however, the growth rate almost equaled to that without nanoparticles, implying that the nanoparticles had ignorable influences on the third and fourth kinetic stages. It is reasonable because the subsequent formation of mature fibrils dominantly occurs between nanoparticle-protein coronas with organized β-sheet-rich structure, leading to fibril-bridged nanoparticle assemblies.

For ThT molecules, surfaces of the protein cross-β structures are their favorite binding sites, where the surface-exposed grooves lined with aromatic amino acids of side chains form extended channel-like motifs, restricting the free rotations of bound benzylamine and benzathiole rings of ThT and enhancing fluorescence intensities [85]. Thus, both ThT fluorescence assay and Raman spectra of the N−Cα−C band intensity at 933 cm^{-1} and the amide I band undoubtedly confirm that AgNPs dominantly play a bridge role in the secondary-structure transformation from α-helices to organized β-sheets, in comparison to the thermal and acidic treatment.

E. Action mechanism of AgNPs at different concentrations

As mentioned above, AgNPs have specific influences on each kinetic stage of the HEWL amyloid fibrillation. FIG. 7 shows the action mechanism diagram of AgNPs in amyloid fibrillation kinetics of HEWL under thermal and acidic conditions.

With the addition of the nanoparticles into HEWL aqueous solution, the negative-charged surfaces of spherical AgNPs are instantaneously coated by proteins to form coronas owing to electrostatic interaction. At the low concentration, the electrostatic interaction naturally attracts those positively charged amino acid residues like arginine and lysine, resulting in a mitigation for disulfide bond breaking. Since local hydrophobic residues are generally buried inside the folded protein with disulfide bonds to form a hydrophobic core, the Trp residues on side chains are protected to a certain extent from the exposure to a hydrophilic environment or an aqueous medium [86−89]. In one word, AgNPs play a stabilizer role in the early stage of the HEWL amyloid fibrillation under these conditions. Moreover, with the incubation time, the absorbed proteins on the surfaces of nanoparticles gradually self-assemble. AgNPs exhibit an improvement of HEWL secondary structure transformation, which can be readily explained as a result of the increase of local protein concentration on the surfaces. It is worth noting that the aggregates are dominantly formed with disordered structures, since more than a half of disulfide bonds remain in proteins. Finally, a large number of amorphous aggregates with random coil structures are observed on the surfaces of AgNPs. Therefore, AgNPs present an inhibiting effect on the formation of amyloid fibrils due to promoting amorphous aggregates.

DOI:10.1063/1674-0068/cjcp2104069

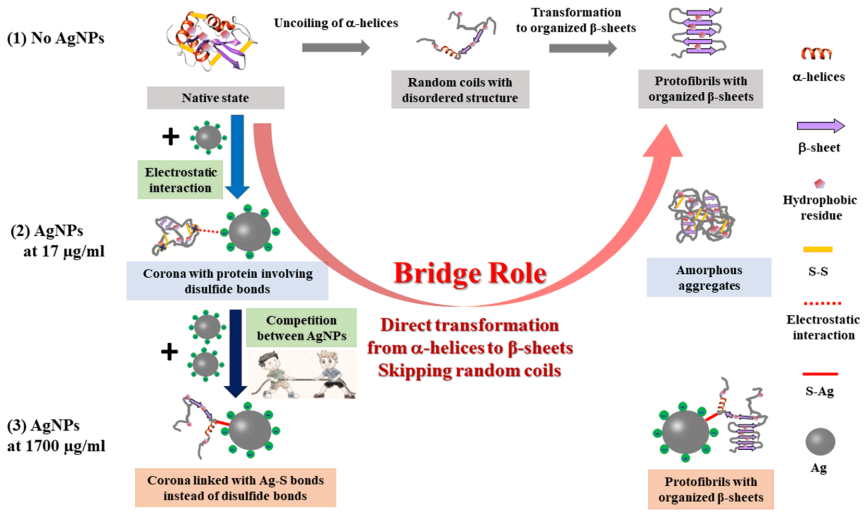

FIG. 7 Action mechanism diagram of Ag nanoparticles in amyloid fibrillation of hen egg-white lysozyme.

In contrast, AgNPs at the high concentration show the entirely different kinetic influences. Upon the addition of nanoparticles into the HEWL solution, the competition among electrostatic interactions from a great deal of nanoparticles will break disulfide bonds to form Ag−S bonds, promoting denaturation of protein. Accompanying the disruption of native disulfide bonds, the hydrophobic residues are exposed to an aqueous environment, preferring the formation of cross β-sheets or β-turns [90, 91]. Thus, the secondary structure transformation of HEWL is naturally accelerated. Specially, according to providing functional surfaces for protein to interact with, AgNPs play a bridge role in transformation from α-helices to organized β-sheets, in comparison to the thermal and acidic treatment. In addition, the nanoparticles do not affect the maturation of protofibrils, in which the most organized β-sheets are formed finally.

IV. CONCLUSION

In this study, we performed a joint study of Raman spectroscopy, AFM and ThT fluorescence assays, to investigate influences of AgNPs at various concentrations on the amyloid fibrillation kinetics of HEWL. The N−Cα−C stretching vibration at 933 cm^{-1}, the amide I band at 1640−1680 cm^{-1}, the Fermi doublet peaks of Trp at 1340 and 1360 cm^{-1}, and the SS stretching band at 507 cm^{-1}, were used to monitor the tertiary and secondary structure changes of protein as well-known Raman indicators, revealing the detailed kinetics of the HEWL amyloid fibrillation at the molecular level.

From the incubation time-dependent Raman spectra, we validated the concentration-dependent influence of AgNPs. In details, this influence was found to be specific for each kinetic stage of the whole amyloid fibrillation. At the early stage, the negative-charged surfaces of nanoparticles are instantaneously coated by proteins to form coronas due to electrostatic interaction, when AgNPs are added into the HEWL aqueous solution. At the low concentration, these coronas are dominantly linked with nanoparticles and those positively charged amino acid residues, thus palliating the disulfide bond breaking and the exposure of hydrophobic residues like Trp to a hydrophilic environment. As a result, the amorphous aggregates are favorable to be formed rather than fibrils, and therefore, AgNPs at the low concentration show an inhibiting effect on the HEWL amyloid fibrillation due to the formation of aggregates with low toxicity. In contrast, at the high concentration, the competition between electrostatic interactions from a great deal of AgNPs induce the breakage of disulfide bonds to form Ag−S bonds, exposing those buried hydrophobic residues and accelerating the formation of cross β-sheets or β-turns structures. Moreover, AgNPs promote the direct transformation from α-helices to organized β-sheets, skipping the formation of random coils. In summary, AgNPs at the high concentration play an efficient accelerator for the HEWL amyloid fibrillation.

Nanoparticle therapeutic carriers are passively targeted to tumors through the enhanced permeability

DOI:10.1063/1674-0068/cjcp2104069

and retention effect, thus they are ideally suited for the delivery of chemotherapeutics in cancer treatment [12]. Thus, the dosage of nanoparticles as a drug carrier should be more considered in the delivery of tumor drugs. In this context, the toxicity of nanoparticle itself at different concentrations to organisms is a subject of concern. Our investigation provides some useful information for developing new medicines for the neurodegenerative diseases and exploring the interactions between proteins and nanoparticles.

Supplementary materials: The UV-visible absorption spectra of AgNPs and SEM image of AgNPs are available.

V. ACKNOWLEDGMENTS

This work was supported by the National Natural Science Foundation of China (No.22073088 and No.21873089).

[1] C. M. Dobson, Nature **426**, 884 (2003).
[2] J. C. Rochet and P. T. Lansbury Jr., Curr. Opin. Struct. Biol. **10**, 60 (2000).
[3] F. Chiti and C. M. Dobson, Annu. Rev. Biochem. **75**, 333(2006).
[4] V. N. Uversky and A. L. Fink, Biochim. Biophys. Acta **1698**, 131 (2004).
[5] C. M. Dobson, Semin. Cell Dev. Biol. **15**, 3 (2004).
[6] S. Bhattacharya, S. Ghosh, S. Dasgupta, and A. Roy, Spectrochim. Acta Part A **114**, 368 (2013).
[7] W. Wang, S. Nema, and D. Teagarden, Int. J. Pharm. **390**, 89 (2010).
[8] S. Ghasemzadeh, and G. H. Riazi, Int. J. Biol. Macromol. **154**, 1505 (2020).
[9] W. Fan, L. Xing, N. Chen, X. Zhou, Y. Yu, and S. Liu, J. Phys. Chem. B **123**, 8057 (2019).
[10] L. Jin, W. Gao, C. Liu, N. Zhang, S. Mukherjee, R. Zhang, H. Dong, A. Bhunia, Z. Bednarikova, Z. Gazova, M. Liu, J. Han, and H. C. Siebert, Int. J. Biol. Macromol. **161**, 1393 (2020).
[11] A. Sakalauskas, M. Ziaunys, and V. Smirnovas, Sci. Rep. **10**, 14466 (2020).
[12] A. Z. Wang, R. Langer, and O. C. Farokhzad, Annu. Rev. Med. **63**, 185 (2012).
[13] T. M. M. Ways, K. W. Ng, W. M. Lau, and V. V. Khutoryanskiy, Pharmaceutics **12**, 751(2020).
[14] M. Manzano and M. Vallet-Regí, Adv. Funct. Mater. **30**, 1902634 (2019).
[15] D. R. Janagam, L. Wu, and T. L. Lowe, Adv. Drug. Deliv. Rev. **122**, 31 (2017).
[16] T. Cedervall, I. Lynch, S. Lindman, T. Berggard, E. Thulin, H. Nilsson, K. A. Dawson, and S. Linse, Proc. Natl. Acad. Sci. USA **104**, 2050 (2007).
[17] M. Lundqvist, J. Stigler, G. Elia, I. Lynch, T. Cedervall, and K. A. Dawson, Proc. Natl. Acad. Sci. USA **105**, 14265 (2008).
[18] I. Lynch and K. A. Dawson, Nano Today **3**, 40 (2008).
[19] B. G. Anand, K. Dubey, D. S. Shekhawat, and K. Kar, Biochemistry **55**, 3345 (2016).
[20] M. Barbalinardo, A. Antosova, M. Gambucci, Z. Bednarikova, C. Albonetti, F. Valle, P. Sassi, L. Latterini, Z. Gazova, and E. Bystrenova, Nano Res. **13**, 1081 (2020).
[21] A. Andrea, B. Zuzana, K. Martina, A. Iryna, M. Jozef, K. Martina, Z. Vlasta, J. Alena, and G. Zuzana, Chem. Eur. J. **25**, 7501 (2019).
[22] R. Vácha, S. Linse, and M. Lund, J. Am. Chem. Soc. **136**, 11776 (2014).
[23] S. Sardar, M. Anas, S. Maity, S. Pal, H. Parvej, S. Begum, R. Dalui, N. Sepay, and U. C. Halder, Int. J. Biol. Macromol. **125**, 596 (2019).
[24] M. Wang, A. Kakinen, E. H. Pilkington, T. P. Davis, and P. C. Ke, Biomater. Sci. **5**, 485 (2017).
[25] A. Gladytz, M. Wagner, T. Haupl, C. Elsner, and B. Abel, Part. Part. Syst. Charact. **32**, 573 (2015).
[26] P. Nedumpully-Govindan, E. N. Gurzov, P. Chen, E. H. Pilkington, W. J. Stanley, S. A. Litwak, T. P. Davis, P. C. Ke, and F. Ding, Phys. Chem. Chem. Phys. **18**, 94 (2016).
[27] L. Bellucci, A. Ardevol, M. Parrinello, H. Lutz, H. Lu, T. Weidner, and S. Corni, Nanoscale **8**, 8737 (2016).
[28] S. Auer, A. Trovato, M. Vendruscolo, and G. Hummer, PLoS Comput. Biol. **5**, 1000458 (2009).
[29] C. Elsner, D. Hintzen, A. Prager, K. R. Siefermann, and B. Abel, Z. Phys. Chem. **229**, 427 (2015).
[30] Y. H. Liao, Y. J. Chang, Y. Yoshiike, Y. C. Chang, and Y. R. Chen, Small **8**, 3631 (2012).
[31] C. Cabaleiro-Lago, O. Szczepankiewicz, and S. Linse, Langmuir **28**, 1852 (2012).
[32] H. He, J. E. Ostwaldt, C. Hirschhauser, C. Schmuck, and J. Niemeyer, Small **16**, 2001044 (2020).
[33] J. Zhang, L. Mou, and X. Jiang, Chem. Sci. **11**, 923 (2020).
[34] N. Sorout and A. Chandra, J. Phys. Chem. B **124**, 1928 (2020).
[35] T. John, A. Gladytz, C. Kubeil, L. L. Martin, H. J. Risselada, and B. Abel, Nanoscale **10**, 20894 (2018).
[36] B. Meesaragandla, S. Karanth, U. Janke, and M. Delcea, Sci. Rep. **10**, 7862 (2020).
[37] B. Ma, F. Zhang, X. Wang, and X. Zhu, Int. J. Biol. Macromol. **98**, 717 (2017).
[38] Y. Zou, W. Hao, H. Li, Y. Gao, Y. Sun, and G. Ma, J. Phys. Chem. B. **118**, 9834 (2014).

DOI:10.1063/1674-0068/cjcp2104069

[39] E. Frare, P. Polverino De Laureto, J. Zurdo, C. M. Dobson, and A. Fontana, J. Mol. Biol. **340**, 1153 (2004).
[40] D. R. Booth, M. Sunde, V. Bellotti, C. V. Robinson, W. L. Hutchinson, P. E. Fraser, P. N. Hawkins, C. M. Dobson, S. E. Radford, C. C. F. Blake, and M. B. Pepys., Nature **385**, 787 (1997).
[41] D. Kumar Ban, and S. Paul, Appl. Surf. Sci. **473**, 373 (2019).
[42] R. Hassan, M. Azam-Sadat, M. Nasrin, and K. Reza, J. Iran. Chem. Soc. **16**, 33 (2019).
[43] J. Turkevich, P. C. Stevenson, and J. Hillier, Discuss. Faraday Soc. **11**, 55 (1951).
[44] S. Al Gharib, J. L. Marignier, A. K. El Omar, A. Naja, S. Le Caer, M. Mostafavi, and J. Belloni, J. Phys. Chem. C **123**, 22624 (2019).
[45] P. C. Lee and D. Meisel, J. Phys. Chem. **86**, 3391 (1982).
[46] S. Agnihotri, S. Mukherji, and S. Mukherji, RSC Adv. **4**, 3974 (2014).
[47] R. Swaminathan, V. K. Ravi, S. Kumar, M. V. Kumar, and N. Chandra, Adv. Protein Chem. Struct. Biol. **84**, 63 (2011).
[48] V. A. Shashilov and I. K. Lednev, J. Am. Chem. Soc. **130**, 309 (2008).
[49] L. Xing, W. Fan, N. Chen, M. Li, X. Zhou, and S. Liu, J. Raman Spectrosc. **50**, 629 (2019).
[50] R. Majumdar, P. Manikwar, J. M. Hickey, H. S. Samra, H. A. Sathish, S. M. Bishop, C. R. Middaugh, D. B. Volkin, and D. D. Weis, Biochemistry **52**, 3376 (2013).
[51] Y. Zhang and P. S. Cremer, Proc. Natl. Acad. Sci. **106**, 15249 (2009).
[52] V. N. Uversky J. Li, and A. L. Fink, J. Biol. Chem. **276**, 44284 (2001).
[53] K. Lin, X. G. Zhou, S. L. Liu, and Y. Luo, Chin. J. Chem. Phys. **26**, 121 (2013).
[54] L. Chen, W. Zhu, K. Lin, N. Hu, Y. Yu, X. Zhou, L. F. Yuan, S. M. Hu, and Y. Luo, J. Phys. Chem. A **119**, 3209 (2015).
[55] Y. Yu, W. Fan, Y. Wang, X. Zhou, J. Sun, and S. Liu, Sensors **18**, 2061 (2018).
[56] Y. Yu, W. Fan, Y. Wang, X. Zhou, J. Sun, and S. Liu, J. Phys. Chem. B **121**, 8179 (2017).
[57] X. Chen, W. Fan, X. Zhou, and S. Liu, Chin. J. Chem. Phys. **32**, 553 (2019).
[58] L. Xing, N. Chen, W. Fan, M. Li, X. Zhou, and S. Liu, Int. J. Biol. Macromol. **132**, 929 (2019).
[59] L. Xing, K. Lin, X. Zhou, S. Liu, and Y. Luo, J. Phys. Chem. B **120**, 10660 (2016).
[60] V. Kocherbitov, J. Latynis, A. Misiunas, J. Barauskas, and G. Niaura, J. Phys. Chem. B **117**, 4981 (2013).
[61] A. Tinti, M. Di Foggia, P. Taddei, A. Torreggiani, M. Dettin, and C. Fagnano, J. Raman Spectrosc. **39**, 250 (2008).
[62] B. Frushour and J. Koenig, Biopolymers **13**, 1809(1974).
[63] B. Frushour and J. Koenig, Biopolymers **14**, 649 (1975).
[64] A. Rygula, K. Majzner, K. M. Marzec, A. Kaczor, M. Pilarczyk, and M. Baranska, J. Raman Spectrosc. **44**, 1061(2013).
[65] T. G. Spiro and B. P. Gaber, Annu. Rev. Biochem. **46**, 553 (1977).
[66] V. A. Shashilov and I. K. Lednev, J. Am. Chem. Soc. **130**, 309 (2008).
[67] M. Xu, V. Shashilov and I. K. Lednev, J. Am. Chem. Soc. **129**, 11002 (2007).
[68] V. A. Shashilov, M. Xu, V. V. Ermolenkov, and I. K. Lednev, J. Quant. Spectrosc. Radiat. Transfer. **102**, 46(2006).
[69] Z. Q. Wen, J. Pharm. Sci. **96**, 2861(2007).
[70] H. Sugeta, A. Go, and T. Miyazawa, Bull. Chem. Soc. Jpn. **46**, 3407(1973).
[71] N. Howell and E. Li-Chan, Int. J. Food Sci. Technol. **31**, 439 (2010).
[72] A. M. Herrero, P. Carmona, S. Cofrades, and F. Jimenez-Colmenero, Food. Res. Int. **41**, 765 (2008).
[73] A. M. Herrero, M. I. Cambero, J. A. Ordonez, L. de la Hoz, and P. Carmona, Food. Chem. **109**, 25 (2008).
[74] M. V. Trivedi, J. S. Laurence, and T. J. Siahaan, Curr. Protein Pept. Sci. **10**, 614 (2009).
[75] R. Honda, T. Gyobu, H. Shimahara, Y. Miura, and Y. Hoshino, ACS Appl. Bio. Mater. **3**, 3827 (2020).
[76] Y. Bu and S. Lee, ACS Appl. Mater. Interfaces. **4**, 3923 (2012).
[77] R. A. Alvarez-Puebla, E. Arceo, P. J. G. Goulet, J. J. Garrido, and R. F. Aroca, J. Phys. Chem. B **109**, 3787 (2005).
[78] D. Joshi, and R. K. Soni, Appl. Phys. A **116**, 635 (2014).
[79] L. Marino, K. Pauwels, R. Casasnovas, P. Sanchis, B. Vilanova, F. Munoz, J. Donoso, and M. Adrover, Sci. Rep. **5**, 12052 (2015).
[80] I. Harada, T. Miura, and H. Takeuchi, Spectrochim. Acta Part A **42**, 307 (1986).
[81] L. A. Popova, R. Kodali, R. Wetzel, and I. K. Lednev, J. Am. Chem. Soc. **132**, 6324 (2010).
[82] I. W. Hamley, Angew. Chem. Int. Ed. Engl. **46**, 8128 (2007).
[83] H. LeVine, Methods Enzymol **309**, 274 (1999).
[84] H. Levine, Protein Sci. **2**, 404 (1993).
[85] M. Biancalana and S. Koide, Biochim. Biophys. Acta **1804**, 1405 (2010).
[86] V. Wineman-Fisher, L. Tudorachi, E. Nissim, and Y. Miller, Phys. Chem. Chem. Phys. **18**, 12438 (2016).
[87] Y. Li, J. Yan, X. Zhang, and K. Huang, Proteins **81**, 1862 (2013).
[88] Y. Harpaz, M. Gerstein, and C. Chothia, Structure **2**,

DOI:10.1063/1674-0068/cjcp2104069

641 (1994).
[89] W. J. Wedemeyer, E. Welker, M. Narayan, and H. A. Scheraga, Biochemistry **39**, 4207 (2000).
[90] B. Ahmad, J. Winkelmann, B. Tiribilli, and F. Chiti, Biochim. Biophys. Acta **1804**, 223 (2010).
[91] J. C. Rochet, Expert Rev. Mol. Med. **9**, 1 (2007).

DOI:10.1063/1674-0068/cjcp2104069